Next Energy 1 (2023) 100048

Contents lists available at ScienceDirect

Next Energy

journal homepage: www.sciencedirect.com/journal/next-energy

Interface coordination regulation of zinc ions for advanced zinc-iodine batteries

Yadong Tian [a], Song Chen [a], Qianwu Chen [a], Siyu Ding [a], Kwan San Hui [b], Jintao Zhang [a,*]

[a] Key Laboratory for Colloid and Interface Chemistry, Ministry of Education, School of Chemistry and Chemical Engineering, Shandong University, Jinan 250100, China
[b] School of Engineering, Faculty of Science, University of East Anglia, Norwich NR4 7TJ, United Kingdom

ARTICLE INFO

Keywords:
Interface regulation
Zinc-iodine battery
Coordination
Rechargeable battery

ABSTRACT

Aqueous rechargeable zinc-iodine batteries, as an alternative to lithium-ion batteries (LIBs), deliver the advantages of high theoretical specific capacity, high safety, environmental friendliness, and abundant reserves, making them suitable for large-scale energy storage applications. Nevertheless, unstable Zn anodes would cause a series of symptoms, such as the growth of Zn dendrites and side reactions, which endanger the stability and lifespan of the batteries. Herein, an organic-metal (PAA-Zn) functional film is introduced onto the surface of Zn foil via the coordination of polyacrylic acid and divalent ions to address the above challenges of Zn anodes. The PAA-Zn functional films adjust the uniform distribution of the interfacial electric field, which is advantageous for uniform Zn plating/stripping. Additionally, the abundant oxygen-containing functional groups not only significantly enhance the interfacial hydrophilicity, but also reduce the number of free water molecules reaching the Zn foil surface through the isolation and desolvation effect of functional groups, thus inhibiting corrosion and hydrogen evolution side reactions. As a result, PAA-Zn electrodes exhibited a stable cycling for over 1000 h in symmetrical cells. Most importantly, the Zn-I_2 batteries demonstrated a high specific capacity with a retention rate of 89.9 % during 3500 cycles when assembled with PAA-Zn anodes.

Introduction

Aqueous rechargeable zinc-iodine batteries are the new stars of next-generation energy storage devices due to their natural advantages, such as high flame retardance, high theoretical specific capacity, abundant reserves, and environmental friendliness [1–7]. However, the notorious Zn dendrites formed during Zn plating/stripping greatly threaten the safety and stability of zinc-iodine batteries [8,9]. Corrosion, hydrogen evolution, and other side reactions inevitably occur and produce insulating corrosion products (e.g., $Zn_4SO_4(OH)_6{\cdot}xH_2O$) due to the thermodynamic instability of metallic Zn in weak acidic aqueous electrolyte [10,11]. Additionally, the hydrogen evolution reaction, as a competitive reaction to zinc deposition during the Zn plating/stripping process, leads to low coulombic efficiency and a continuous increase in internal battery pressure [12,13]. Therefore, finding a practical and effective strategy to improve the stability of Zn anodes by inhibiting dendrites and harmful side reactions is urgently needed for the development of high-performance zinc-iodine batteries.

Currently, a series of advanced strategies has been proposed to improve the stability of Zn anodes, such as interface modification layers [14,15], electrolyte additives [16,17], three-dimensional electrode structure design [18,19], and other effective strategies. For example, 3D porous carbon material has been used as a zincophilic host to fabricate 3D porous Zn anodes for inhibiting dendrite growth [20]. The 3D porous structure and high zinc affinity of the carbon material facilitate rapid electron/ion transport and guide uniform Zn deposition. Although 3D Zn anodes can reduce local current density and alleviate dendrite growth, the complex production process and high cost make them unsuitable for large-scale energy storage equipment [21]. Interface modification layer is a promising and effective solution due to their simple preparation process and potential for large-scale production [22,23]. An artificial polyamine (PDA) interface layer has been developed to improve the stability of Zn anodes [24]. The PDA layer offers dual functions of fast desolvation and ion confinement, which inhibit the hydrogen evolution reaction and dendrite growth [25]. Furthermore, the zinc oxalate interface layer (Zn@ZCO) with nucleophilic carbonyl groups has been constructed spontaneously as the ion screening and functional protective layer to improve the stability of zinc anodes [26]. The carbonyl oxygen exhibits strong nucleophilicity when coordinating with zinc ions, which is conducive to ion transport, thus effectively

* Corresponding author.
E-mail address: jtzhang@sdu.edu.cn (J. Zhang).

https://doi.org/10.1016/j.nxener.2023.100048
Received 25 June 2023; Received in revised form 9 August 2023; Accepted 14 August 2023
Available online 25 August 2023

regulating the uniform zinc deposition to inhibit dendrite formation. However, some interface layers may increase interface impedance due to poor compatibility and hinder ion transmission. Currently, most reports in the literature focus on inorganic interface layers, with limited research on polymer interface layers, mostly carried out at low current densities [27]. Therefore, further study is necessary.

In this study, a uniform PAA-Zn functional film was obtained on the surface of Zn foil by coordinating polyacrylic acid and divalent ions to improve the stability of Zn anodes. The carboxylate groups uniformly distributed in the PAA-Zn film adjust the electric field distribution at the interface, inhibiting the growth of Zn dendrites. Additionally, the abundant oxygen-containing functional groups significantly enhance interfacial hydrophilicity and improve electrolyte/electrode interface contact. The hydrophilic PAA-Zn film would reduce the amount of free water molecules reaching to the surface of Zn foil by isolating and desolvation effect of functional groups, inhibiting corrosion and hydrogen evolution side reactions. As expected, symmetrical cells assembled with PAA-Zn anodes showed a long cycling lifespan of over 1000 h with excellent stability. Even at a high current density of 5 mA cm^{-2}, PAA-Zn anodes maintained stable cycling for over 500 h in symmetrical cells. More importantly, the Zn-iodine batteries with PAA-Zn anodes exhibited a high initial specific capacity of 215.9 mAh g^{-1} with a high capacity retention rate (89.9 %) during 3500 cycles.

Results and discussion

It is a common phenomenon that metal deposition morphology tends to form dendrites, which is generally observed in various metal batteries [28,29]. Zinc ions tend to preferentially deposit at the positions with high surface energy due to the uneven distribution of the interface electric field and concentration gradient, resulting in dendrite growth [30,31]. To address dendrite growth caused by the tip effect, a multifunctional PAA-Zn film was fabricated through the coordination of polyacrylic acid with Zn ions. As shown in Fig. 1, PAA-Zn functional films formed on the surface of Zn foil through the coordination of PAA and zinc ions. The uneven Zn deposition on the surface of Zn foils usually leads to the growth of dendrites during the charging and discharging processes, which would eventually cause dendrites to penetrate the

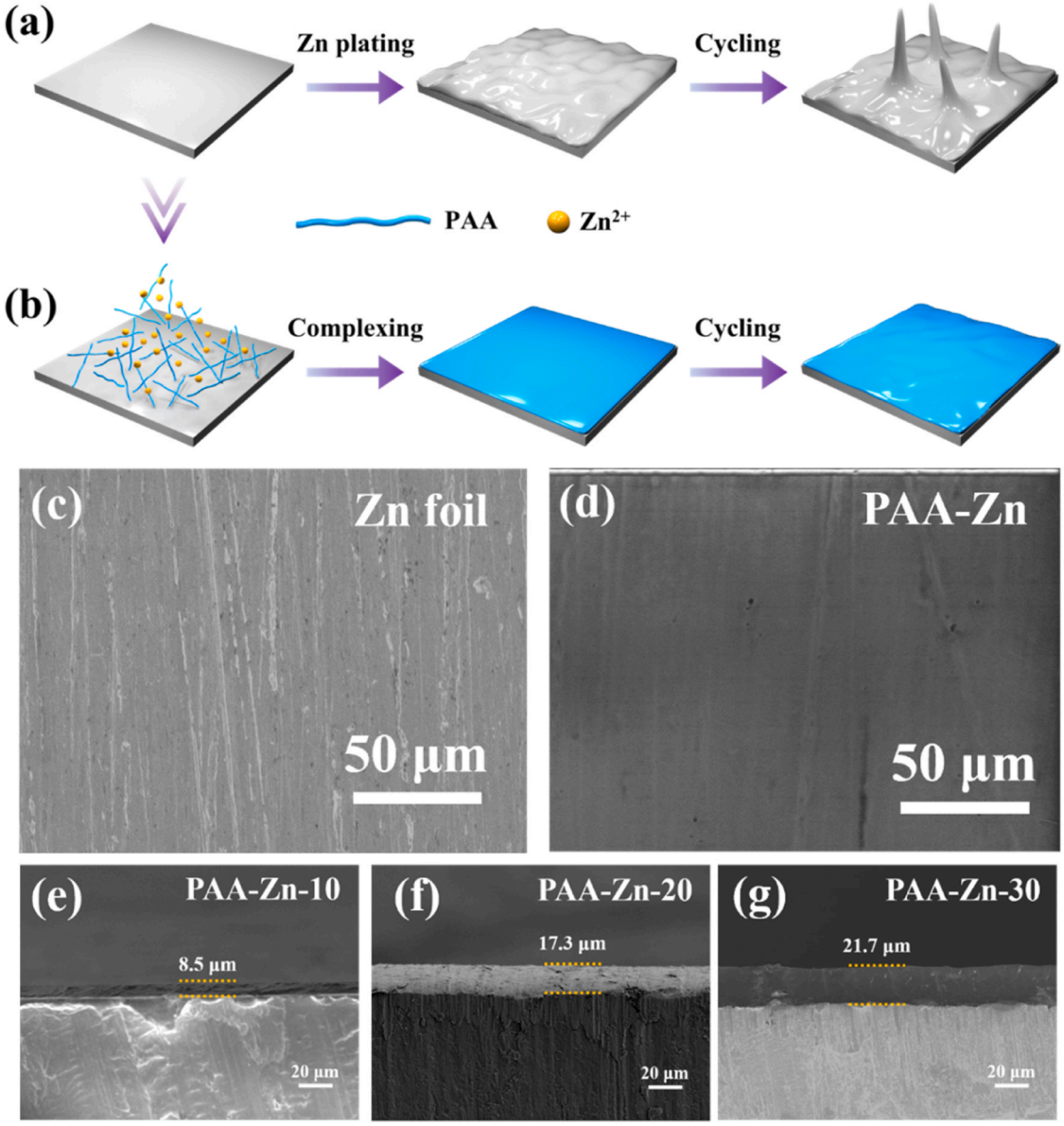

Fig. 1. Schematic illustrations of the PAA-Zn functional films fabrication process and the behavior of (a) Zn foil and (b) PAA-Zn electrode during cycling. SEM images of (c) Zn foil and (d) PAA-Zn. Cross-sectional SEM images of (e) PAA-Zn-10, (f) PAA-Zn-20 and (g) PAA-Zn-30.

separators and create short circuits (Fig. 1a) [32,33]. In contrast, the abundant carboxylate groups distributed in the PAA-Zn functional film would adjust the uniform distribution of the electric field at the interface, thus promoting uniform Zn deposition (Fig. 1b) [34]. Additionally, the stable PAA-Zn interface layer can isolate free water molecules, effectively inhibiting hydrogen evolution and corrosion side reactions.

The microscopic morphology of PAA-Zn functional films with different reaction times was observed using scanning electron microscopy (SEM). Compared with zinc foils, PAA-Zn films exhibit uniform and smooth surfaces (Fig. 1c, d). Additionally, PAA-Zn-10 after surface modification also presents a film similar to PAA-Zn-20 (Fig. S1a). In contrast, PAA-Zn-30 shows some small cracks, possibly caused by residual stress due to prolonged reaction time (Fig. S1b) [35,36]. Cross-section SEM images reveal that the thickness of PAA-Zn-T films increases from 8.5 μm (PAA-Zn-10) to 21.7 μm (PAA-Zn-30) with the extension of reaction time (Fig. 1e-g). However, a thicker interface layer is not conducive to ion transport and may result in increased interface impedance. On the other hand, the interface layer should have a certain thickness to handle the morphological fluctuations caused by rapid charging and discharging under high current density. Therefore, the optimal reaction time is determined to be 20 min. Element mapping images show that C, O, and Zn are uniformly distributed on the surface of the Zn foil, indicating the formation of a uniform film structure (Fig. S2a-c).

The surface hydrophilicity of the different electrodes was characterized using a contact angle test. As shown in Fig. 2a, the contact angle between the untreated zinc foil surface and the water drop is 107.8°, indicating poor contact between the Zn foil and the electrolyte. In contrast, PAA-Zn exhibits the smallest contact angle (32.4°), indicating the best hydrophilicity (Fig. 2b). These experimental results illustrate that the PAA-Zn film can significantly improve the surface hydrophilicity by forming abundant hydrogen bonding with water molecules, which is conducive to the transport of Zn ions and the reduction of interface resistance [37,38].

The characterization of PAA-Zn films was analyzed by Fourier transform infrared spectroscopy (FT-IR). As shown in Fig. S3, the absorption peak at 2931 cm^{-1} should be assigned to the -CH_2- or >CH- stretching vibrations in the polymer backbone. The characteristic absorption peak at 1700 cm^{-1} is attributed to the C═O stretching vibrations of the abundant carboxylate functional groups contained in the PAA films (Fig. 2c). In the case of PAA-Zn, the carboxyl band shifts to the lower frequency region (1555 cm^{-1}). This is caused by the addition of Zn ions, forming metal complexes with PAA, which changes the arrangement of carboxyl bands from local C═O bonds (α) to symmetrically ionized structures (β) (Fig. 2d) [39]. This structural change directly leads to the appearance of double states, corresponding to the asymmetric and symmetric stretching vibrations of carboxylate functional groups. Therefore, the absorption peak at 1555 cm^{-1} in the FT-IR spectrum of PAA-Zn is attributed to the asymmetric stretching vibration of -COO- [39]. The new absorption peak at the low wavenumber (1322 cm^{-1}) corresponds to the symmetrical stretching vibration of carboxylate functional groups [39]. The characteristic scissor peaks at 1448 cm^{-1} and 1415 cm^{-1} in the FT-IR spectra are assigned to the bending vibration of -CH_2- or >CH- [39,40]. The above results of the FT-IR spectra indicate that the PAA-Zn functional film was successfully synthesized on the surface of the Zn foil through the formation of metal complexes of polyacrylic acid and Zn ions.

The crystallographic information of PAA-Zn films and corrosion products was characterized by X-ray diffraction (XRD). As shown in Fig. 2e, the XRD pattern of PAA-Zn without other characteristic peaks except for metallic Zn, indicating that the PAA-Zn film is amorphous. Subsequently, PAA-Zn electrode was immersed in 2 M $ZnSO_4$ aqueous

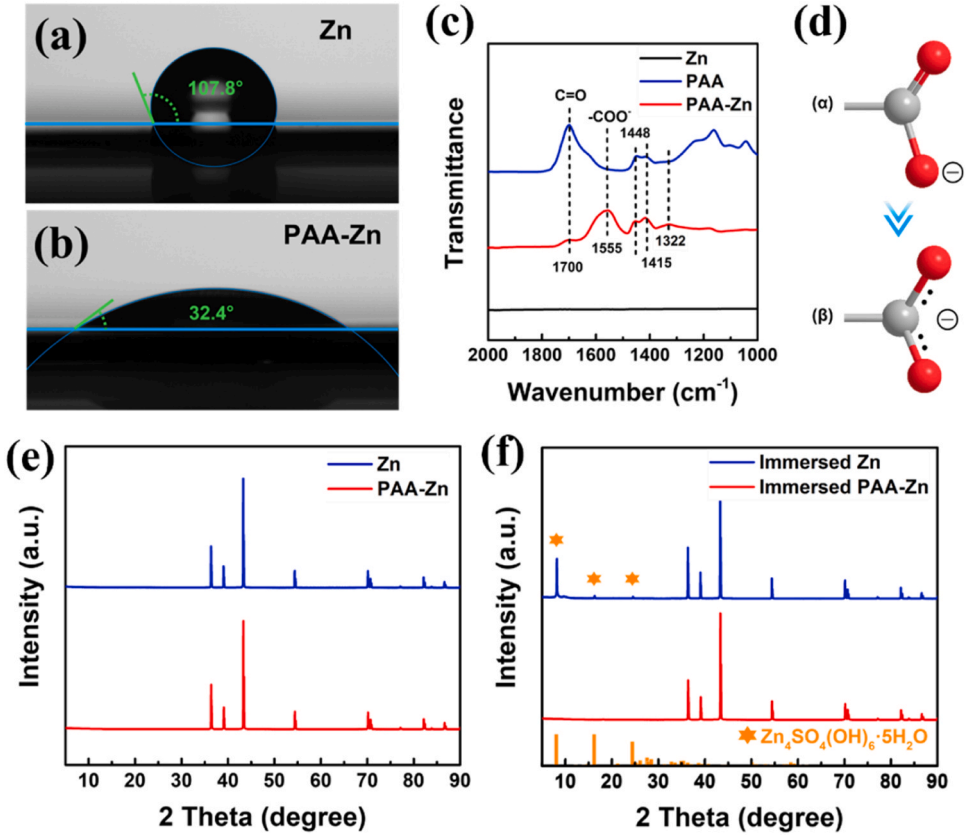

Fig. 2. The contact angle test for (a) Zn and (b) PAA-Zn. (c) FT-IR spectra of pure PAA and PAA-Zn films. (d) Schematic diagram of the transformation of carboxylate group to the symmetrically ionized structure. (e) XRD patterns of PAA-Zn and Zn foil. (f) XRD patterns of PAA-Zn and Zn foil after soaking in 2 M $ZnSO_4$ electrolyte for 5 days.

electrolyte for 5 days to examine the capacity of corrosion resistance. No corrosion products were detected on the surface of the PAA-Zn electrode after immersing in the electrolyte for 5 days, which was consistent with the results of the pristine PAA-Zn (Fig. 2f). In contrast, a strong characteristic peak belonging to $Zn_4SO_4(OH)_6{\cdot}5\,H_2O$ (PDF#39-0688) of corrosion product was detected on the surface of the Zn foil after 5 days of corrosion in the aqueous electrolyte. Moreover, no characteristic peak of corrosion products was detected after cycling test under the protection of the PAA-Zn interface layer in comparison with Zn foil (Fig. S4). The stark contrast in the results illustrates that PAA-Zn functional films

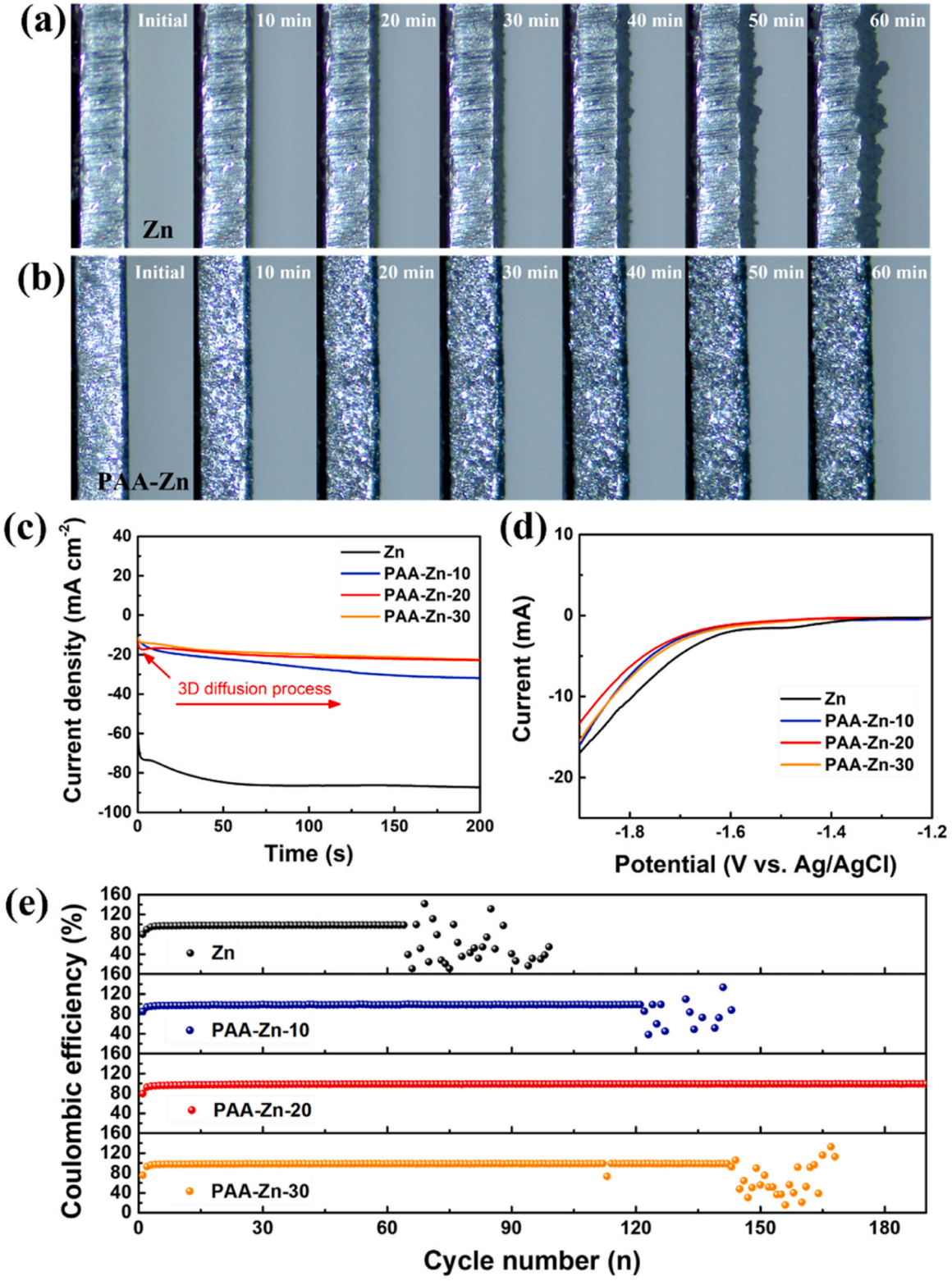

Fig. 3. In situ optical microscope images of (a) Zn foil and (b) PAA-Zn anode during deposition at 10 mA cm^{-2}. (c) Chronoamperometry curves of PAA-Zn-T and Zn foil at a constant potential of − 200 mV. (d) LSV curves of PAA-Zn-T and Zn foil in 1 M Na_2SO_4 aqueous electrolyte with a scan rate of 5 mV s^{-1}. (e) Coulombic efficiency of Zn||CP cells. The cells were assembled with carbon paper and PAA-Zn-T anodes. (f) EIS of PAA-Zn-T.

can promote the desolvation process through the formation of hydrogen bonding by abundant oxygen-containing functional groups, thus effectively inhibiting side reactions and the formation of corrosion products [24,41].

The Zn deposition behavior of PAA-Zn anodes and Zn foils was studied at a high current density of 10 mA cm^{-2} by in situ optical microscopy. As shown in Fig. 3a, the uncontrolled growth of Zn dendrites gradually worsened on the surface of the Zn foil with the extension of deposition time. Eventually, the surface of the Zn foil was covered with a large number of sharp and protruding Zn dendrites, which would pierce the separator and lead to short-circuit. In contrast, the PAA-Zn electrode maintained a flat surface without obvious dendrite formation during the deposition process for 1 h (Fig. 3b). This is attributed to the regulation of the PAA-Zn functional film on the interface electric field, which promotes the formation of a flat deposition layer and inhibits the growth of Zn dendrites.

The deposition behaviors of symmetrical cells assembled with different anodes were revealed by chronoamperometry (CA) at an overpotential of 200 mV. The increase of the deposition response current in the CA curves is caused by dendrite growth, reflecting the degree of dendrites during the deposition process [26,42]. As shown in Fig. 3c, the PAA-Zn symmetrical cells reached the 3D diffusion process in a shorter time due to the adjustment of the PAA-Zn functional film on the interface electric field, thus inhibiting the 2D planar diffusion of Zn^{2+} and achieving uniform Zn deposition. In contrast, the Zn foil exhibited a continuous increase in response current, indicating a long and rampant 2D plane diffusion process in which the Zn ions diffused laterally on the surface and nucleated at the sites with high surface energy, resulting in the continuous growth of dendrites [43,44].

The deposition behavior of Zn on the interface can be further studied by combining with SEM images. As shown in Fig. S4, obvious dendrite growth was observed on the surface of Zn foil, which would lead to poor stability and a reduction in lifespan. In contrast, the PAA-Zn electrode still presented a flat and uniform surface even after cycling for 50 h in symmetrical cells (Fig. S5). The SEM results are consistent with the results of CA curves, which fully indicates that the regulation of PAA-Zn functional film on the interface electric field would guide the uniform Zn deposition, thus inhibiting the dendrite growth.

The hydrogen evolution overpotential is an important parameter to evaluate the corrosion resistance of metal anode. According to the results of the LSV curves, the hydrogen evolution overpotential of PAA-Zn-T electrodes has been improved to varying degrees compared to Zn foils (Fig. 3d). Among them, the optimized sample (PAA-Zn-20) exhibited the highest hydrogen evolution overpotential. The increased hydrogen evolution overpotential indicates that the PAA-Zn functional film can effectively inhibit the hydrogen evolution reaction through the isolation and desolvation effect of functional groups. Electrochemical impedance spectroscopy (EIS) was used to measure the resistance of symmetric cells with PAA-Zn-T anodes. As shown in Fig. S6, the optimized PAA-Zn-20 showed the lowest charge transfer impedance.

Coulombic efficiency of Zn||CP cells with PAA-Zn-T anodes was evaluated at 1 mA cm^{-2} with 1 mAh cm^{-2}. The highly overlapped voltage-capacity curves of PAA-Zn-20 exhibited a high coulombic efficiency and good stability (Fig. S7). As shown in Fig. 3e, Zn||CP cells with PAA-Zn-20 anodes showed stable coulombic efficiency over 190 cycles. However, PAA-Zn-10 and PAA-Zn-30 performed slightly worse, and their coulombic efficiency fluctuated after about 120 cycles. In contrast, the coulombic efficiency of Zn||CP cells assembled with Zn foils was difficult to maintain stable and fluctuated sharply after about 60 cycles. These results indicate that the PAA-Zn film improves the reversibility of Zn plating/stripping, which is attributed to the inhibition of harmful side reactions and dendrites.

According to the detailed voltage profiles, the overpotentials of all PAA-Zn-T anodes were reduced to varying degrees compared with the Zn foil (Fig. 4a). Among them, the PAA-Zn-20 symmetrical cells showed the minimum overpotential, indicating improved reversibility of the Zn anode. As shown in Fig. 4b, the rate performance of the PAA-Zn-T symmetrical cells was measured at current densities ranging from 0.5 to 10 mA cm^{-2}. Obviously, the PAA-Zn-20 symmetrical cells exhibited the lowest voltage hysteresis and a stable voltage distribution, indicating the best rate performance.

Cycling performance of the PAA-Zn-T anodes was measured in

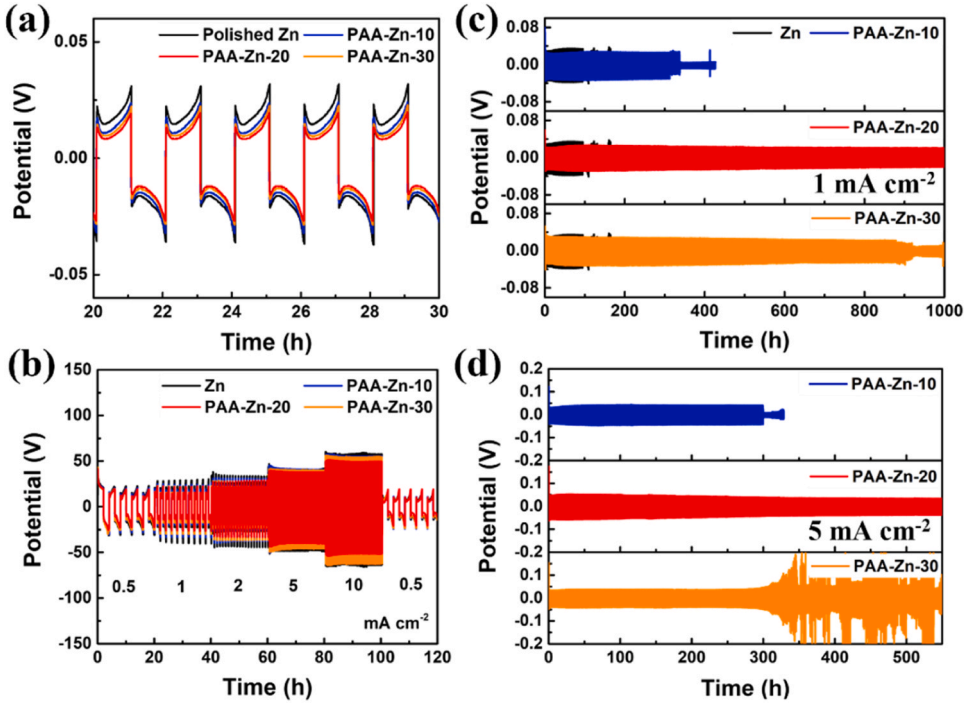

Fig. 4. (a) Detailed voltage profiles of PAA-Zn-T and Zn foil symmetric cells. (b) Rate performances of PAA-Zn-T and Zn foil symmetric cells at current densities from 0.5 to 10 mA cm^{-2}. (c, d) Galvanostatic cycling of PAA-Zn-T electrodes and Zn electrodes in symmetric cells at different current densities with a capacity of 1 mAh cm^{-2}.

symmetric cells under different current densities. As shown in Fig. 4c, the cycling performance of all samples had been significantly enhanced to different degrees compared with the Zn foil. In particular, the symmetric cell with the PAA-Zn-20 anode exhibited stable cycling over 1000 h at 1 mA cm^{-2} with a capacity of 1 mAh cm^{-2}. Even at a larger current density of 5 mA cm^{-2}, the PAA-Zn-20 anode still maintained stable cycling over 500 h in symmetric cells, which is also superior to other PAA-Zn-T electrodes (Fig. 4d). The excellent electrochemical performance and stability of PAA-Zn-20 anodes should be attributed to the appropriate thickness of the interfacial film and the regulation of the interfacial electric field.

The influence of different metal ions on the electrochemical performance was investigated by changing the types of coordination ions. As shown in Fig. S8, the PAA-Mg film and PAA-Mn film displayed many cracks and an uneven surface, which were different from the uniform and flat PAA-Zn film. The surface hydrophilicity of PAA-Mn films was characterized by contact angle test. Obviously, the contact angles of PAA-Mg and PAA-Mn electrodes are 79° and 39°, respectively, which are smaller than those of Zn foils (Fig. S9). Higher hydrophilicity is conducive to the transport of Zn ions and the reduction of interface resistance.

The FT-IR spectrum of PAA-M is similar to that of PAA-Zn. The formation of metal complexes (PAA-M) with different metal ions would lead to the transfer of carboxyl bands to the low-frequency region, which are located at 1573, 1578 and 1555 cm^{-1}, respectively (Fig. S10). From the FT-IR spectrum, it can be concluded that the PAA-M films were successfully fabricated on the surface of Zn foils.

As shown in Fig. S11a, PAA-Mg and PAA-Mn exhibited similar results to Zn foil, indicating a long 2D plane diffusion process, which indicates continuous dendrite growth. The hydrogen evolution overpotential of PAA-M anodes was compared by LSV. As shown in Fig. S11b, PAA-Mg showed a highly overlapping curve with PAA-Zn, indicating that they have similar high hydrogen evolution overpotential. In contrast, PAA-Mn showed a higher response current and better hydrogen evolution performance. In general, PAA-M films reduce the free water molecules reaching the surface of Zn foil through the isolation and desolvation effect of functional groups, thus increasing the hydrogen evolution overpotential of PAA-Zn anodes.

The highly overlapping curves in the voltage distribution profile indicated that there is no significant difference in the overpotential of PAA-M during Zn plating/stripping (Fig. S12a). As shown in Fig. S12b, the rate performance of symmetrical cells with PAA-M was evaluated from 0.5 to 10 mA cm^{-2}. PAA-Zn delivered a smaller overpotential at a high current density of 10 mA cm^{-2}, indicating good rate performance. For cycling performance, PAA-Mg exhibited obvious potential fluctuation after 800 h in symmetrical cells (Fig. S13). Similarly, PAA-Mn showed potential fluctuation after 900 h of cycling, indicating slightly inferior stability compared with PAA-Zn. The uniform PAA-Zn films have favorable hydrophilicity and abundant carboxylate groups, which can reduce the interface impedance and adjust the uniform distribution of the interface electric field, thus achieving outstanding electrochemical performance and stability.

The iodine-loaded PCM-NP [6] (Porous carbon material co-doped with N and P) material was used as the cathodes to assemble the zinc-iodine batteries for further research (Fig. S14). As shown in Fig. 5a, the highly overlapped CV curves suggest that the PAA-Zn functional film has no negative effect on the redox reaction kinetics of iodine with good compatibility. In addition, there is only a pair of redox peaks of iodine without other impurity peaks, indicating that the PAA-Zn film can maintain stability in the entire voltage range of 0.6–1.6 V (Fig. S15) [45]. As shown in Fig. 5b, zinc-iodine batteries assembled with PAA-Zn anodes showed a high specific capacity (218.3 mAh g^{-1}) compared with Zn foil (198.8 mAh g^{-1}) at 1 C. Even at a high rate of 10 C, the zinc-iodine batteries with PAA-Zn still maintained a specific capacity of 166.9 mAh g^{-1}, which was better than zinc foil (147.3 mAh g^{-1}). As shown in Fig. 5c, the zinc-iodine batteries assembled with PAA-Zn exhibited a high specific capacity (215.9 mAh g^{-1}) and high capacity retention rate (89.9 %) with excellent stability during 3500 cycles. In

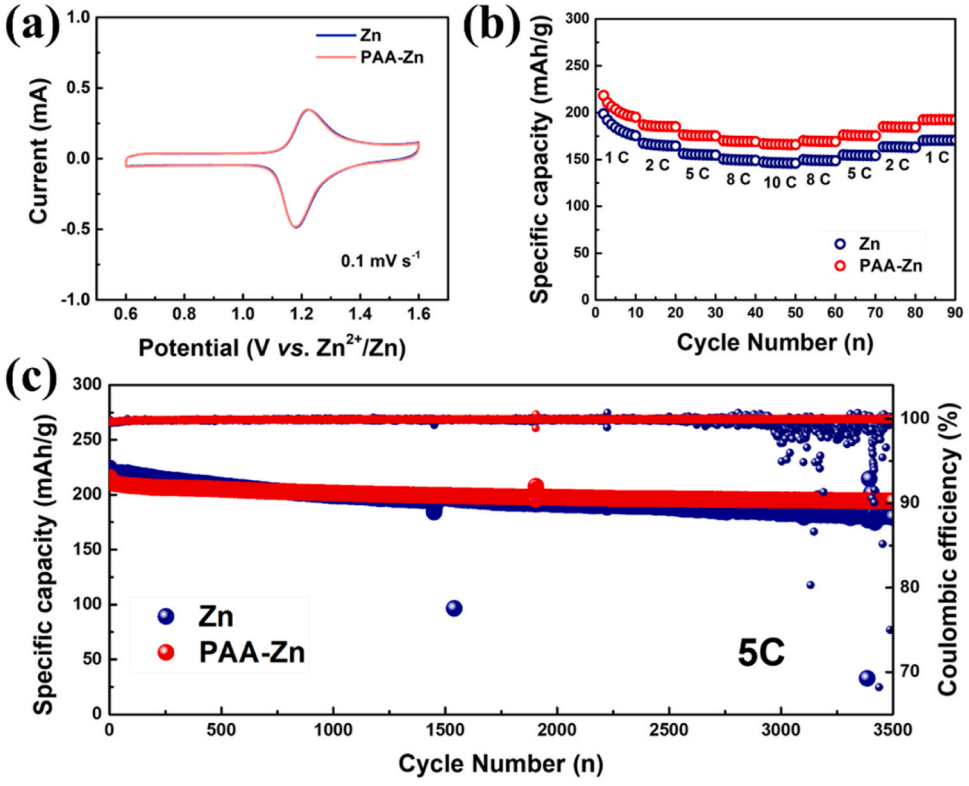

Fig. 5. Comparison of electrochemical performance of PAA-Zn electrode and Zn foil in Zn-I_2 batteries. (a) CV curves. (b) Rate performance from 1 to 10 C. (c) Cycling performance and coulombic efficiency of Zn-I_2 batteries at 5 C.

contrast, the coulombic efficiency of zinc-iodine batteries with Zn foil fluctuated after 2500 cycles, with decreased specific capacity and a lower capacity retention rate (80.2 %). The experimental results illustrate that the PAA-Zn functional films improve the stability of Zn anodes by adjusting the distribution of the electric field at the interface and inhibiting side reactions, thus improving the electrochemical performance of zinc-iodine batteries.

Conclusions

In conclusion, we have developed a strategy of fabricating the organic-metal interface film by coordination to stabilize Zn anodes. The PAA-Zn functional films with distributed carboxylate groups, regulate the uniform distribution of the interface electric field, facilitating uniform Zn deposition. The interfacial hydrophilicity has been significantly improved due to the hydrogen bonding between the PAA-Zn film and water molecules. Additionally, PAA-Zn films effectively inhibit side reactions (corrosion and HER) and the formation of corrosion products through the isolation and desolvation effect of functional groups. As a result, PAA-Zn symmetrical cells have demonstrated a long cycle life of over 1000 h and excellent stability. Importantly, the zinc-iodine batteries incorporating PAA-Zn have exhibited outstanding electrochemical performance and excellent stability over 3500 cycles.

Declaration of Competing Interest

The authors declare that they have no known competing financial interests or personal relationships that could have appeared to influence the work reported in this paper.

Acknowledgements

This work was financially supported by the National Natural Science Foundation of China (22175108), the Natural Scientific Foundation (ZR2020JQ09), the Taishan Scholars Program of Shandong Province, and the Project for Scientific Research Innovation Team of Young Scholars in Colleges, Universities of Shandong Province (2019KJC025). The authors also acknowledge the assistance of the Analytical Center for Structural Constituent and Physical Property of Core Facilities Sharing Platform, Shandong University.

Appendix A. Supporting information

Supplementary data associated with this article can be found in the online version at doi:10.1016/j.nxener.2023.100048.

References

[1] Z. Li, X. Wu, X. Yu, S. Zhou, Y. Qiao, H. Zhou, S.G. Sun, Long-life aqueous Zn-I_2 battery enabled by a low-cost multifunctional zeolite membrane separator, Nano Lett. 22 (6) (2022) 2538–2546, https://doi.org/10.1021/acs.nanolett.2c00460.

[2] S. Chai, J. Yao, Y. Wang, J. Zhu, J. Jiang, Mediating iodine cathodes with robust directional halogen bond interactions for highly stable rechargeable Zn-I_2 batteries, Chem. Eng. J. 439 (2022), 135676, https://doi.org/10.1016/j.cej.2022.135676.

[3] K. Wang, J.-B. Le, S.-J. Zhang, W.-F. Ren, J.-M. Yuan, T.-T. Su, B.-Y. Chi, C.-Y. Shao, R.-C. Sun, A renewable biomass-based lignin film as an effective protective layer to stabilize zinc metal anodes for high-performance zinc-iodine batteries, J. Mater. Chem. A 10 (9) (2022) 4845–4857, https://doi.org/10.1039/d1ta10170f.

[4] H.X. Dang, A.J. Sellathurai, D.P.J. Barz, An ion exchange membrane-free, ultrastable zinc-iodine battery enabled by functionalized graphene electrodes, Energy Storage Mater. 55 (2023) 680–690, https://doi.org/10.1016/j.ensm.2022.12.033.

[5] X. Jin, L. Song, C. Dai, Y. Xiao, Y. Han, X. Li, Y. Wang, J. Zhang, Y. Zhao, Z. Zhang, N. Chen, L. Jiang, L. Qu, A FLexible Aqueous Zinc-iodine Microbattery witH Unprecedented Energy Density, Adv. Mater. 34 (15) (2022), 2109450, https://doi.org/10.1002/adma.202109450.

[6] Y. Tian, S. Chen, Y. He, Q. Chen, L. Zhang, J. Zhang, A highly reversible dendrite-free Zn anode via spontaneous galvanic replacement reaction for advanced zinc-iodine batteries, Nano Res. Energy 1 (3) (2022), e9120025.

[7] M. Wang, Y. Meng, K. Li, T. Ahmad, N. Chen, Y. Xu, J. Sun, M. Chuai, X. Zheng, Y. Yuan, Toward dendrite-free and anti-corrosion Zn anodes by regulating a bismuth-based energizer, eScience 2 (5) (2022) 509–517.

[8] W. Hu, J. Ju, N. Deng, M. Liu, W. Liu, Y. Zhang, L. Fan, W. Kang, B. Cheng, Recent progress in tackling Zn anode challenges for Zn ion batteries, J. Mater. Chem. A 9 (46) (2021) 25750–25772, https://doi.org/10.1039/d1ta08184e.

[9] X. Xu, M. Song, M. Li, Y. Xu, L. Sun, L. Shi, Y. Su, C. Lai, C. Wang, A novel bifunctional zinc gluconate electrolyte for a stable Zn anode, Chem. Eng. J. 454 (2023), 140364, https://doi.org/10.1016/j.cej.2022.140364.

[10] T. Wei, X. Zhang, Y. Ren, Y. Wang, Z. Li, H. Zhang, L. Hu, Reconstructing anode/electrolyte interface and solvation structure towards high stable zinc anode, Chem. Eng. J. 457 (2023), 141272, https://doi.org/10.1016/j.cej.2023.141272.

[11] H. Jia, Z. Wang, B. Tawiah, Y. Wang, C.-Y. Chan, B. Fei, F. Pan, Recent advances in zinc anodes for high-performance aqueous Zn-ion batteries, Nano Energy 70 (2020), 104523, https://doi.org/10.1016/j.nanoen.2020.104523.

[12] J. Yin, X. Feng, Z. Gan, Y. Gao, Y. Cheng, X. Xu, From anode to cell: synergistic protection strategies and perspectives for stabilized Zn metal in mild aqueous electrolytes, Energy Storage Mater. 54 (2023) 623–640, https://doi.org/10.1016/j.ensm.2022.11.006.

[13] T.C. Li, D. Fang, J. Zhang, M.E. Pam, Z.Y. Leong, J. Yu, X.L. Li, D. Yan, H.Y. Yang, Recent progress in aqueous zinc-ion batteries: a deep insight into zinc metal anodes, J. Mater. Chem. A 9 (10) (2021) 6013–6028, https://doi.org/10.1039/d0ta09111a.

[14] X. Lu, C. Zhao, A. Chen, Z. Guo, N. Liu, L. Fan, J. Sun, N. Zhang, Reducing Zn-ion concentration gradient by SO_4^{2-}-immobilized interface coating for dendrite-free Zn anode, Chem. Eng. J. 451 (2023), 138772, https://doi.org/10.1016/j.cej.2022.138772.

[15] X. Zhou, R. Chen, E. Cui, Q. Liu, H. Zhang, J. Deng, N. Zhang, C. Xie, L. Xu, L. Mai, A novel hydrophobic-zincophilic bifunctional layer for stable Zn metal anodes, Energy Storage Mater. 55 (2023) 538–545, https://doi.org/10.1016/j.ensm.2022.12.019.

[16] W. Zhang, Y. Dai, R. Chen, Z. Xu, J. Li, W. Zong, H. Li, Z. Li, Z. Zhang, J. Zhu, F. Guo, X. Gao, Z. Du, J. Chen, T. Wang, G. He, I.P. Parkin, Highly reversible zinc metal anode in a dilute aqueous electrolyte enabled by a pH buffer additive, Angew. Chem. Int. Ed. 62 (5) (2023), e202212695, https://doi.org/10.1002/anie.202212695.

[17] X. Yang, W. Li, Z. Chen, M. Tian, J. Peng, J. Luo, Y. Su, Y. Zou, G. Weng, Y. Shao, S. Dou, J. Sun, Synchronous dual electrolyte additive sustains Zn metal anode with 5600h lifespan, Angew. Chem. Int. Ed. 62 (10) (2023), e202218454, https://doi.org/10.1002/anie.202218454.

[18] G. Li, X. Wang, S. Lv, J. Wang, W. Yu, X. Dong, D. Liu, In situ constructing a film-coated 3D porous Zn anode by iodine etching strategy toward horizontally arranged dendrite-free Zn deposition, Adv. Funct. Mater. 33 (4) (2022), 2208288, https://doi.org/10.1002/adfm.202208288.

[19] Z. Kang, C. Wu, L. Dong, W. Liu, J. Mou, J. Zhang, Z. Chang, B. Jiang, G. Wang, F. Kang, C. Xu, 3D porous copper skeleton supported zinc anode toward high capacity and long cycle life zinc ion batteries, ACS Sustain. Chem. Eng. 7 (3) (2019) 3364–3371, https://doi.org/10.1021/acssuschemeng.8b05568.

[20] P. Xue, C. Guo, N. Wang, K. Zhu, S. Jing, S. Kong, X. Zhang, L. Li, H. Li, Y. Feng, W. Gong, Q. Li, Synergistic manipulation of Zn^{2+}ion flux and nucleation induction effect enabled by 3D hollow SiO_2/TiO_2/carbon fiber for long-lifespan and dendrite-free Zn-metal composite anodes, Adv. Funct. Mater. 31 (50) (2021), 2106417, https://doi.org/10.1002/adfm.202106417.

[21] Q. Cao, Z. Pan, Y. Gao, J. Pu, G. Fu, G. Cheng, C. Guan, Stable imprinted zincophilic Zn anodes with high capacity, Adv. Funct. Mater. 32 (41) (2022), 2205771, https://doi.org/10.1002/adfm.202205771.

[22] P. Wang, B. Sun, X. Wei, L. Yang, H. Wu, Stimulating Zn^{2+} permselectivity for prominent zinc anode reversibility by designing a self-assembled artificial layer, Chem. Eng. J. 455 (2023), 140827, https://doi.org/10.1016/j.cej.2022.140827.

[23] H. Du, R. Zhao, Y. Yang, Z. Liu, L. Qie, Y. Huang, High-capacity and long-life zinc electrodeposition enabled by a self-healable and desolvation shield for aqueous zinc-ion batteries, Angew. Chem. Int. Ed. 61 (10) (2022), e202114789, https://doi.org/10.1002/anie.202114789.

[24] T. Wang, P. Wang, L. Pan, Z. He, L. Dai, L. Wang, S. Liu, S.C. Jun, B. Lu, S. Liang, J. Zhou, Stabling zinc metal anode with polydopamine regulation through dual effects of fast desolvation and ion confinement, Adv. Energy Mater. 13 (5) (2022), 2203523, https://doi.org/10.1002/aenm.202203523.

[25] J. Li, Z. Zheng, Z. Yu, F. She, L. Lai, J. Prabowo, W. Lv, L. Wei, Y. Chen, Stable Zn electrodes enabled by an ultra-thin Zn phosphate protective layer, J. Mater. Chem. A 11 (6) (2023) 3051–3059, https://doi.org/10.1039/d2ta09153d.

[26] P. Wang, S. Liang, C. Chen, X. Xie, J. Chen, Z. Liu, Y. Tang, B. Lu, J. Zhou, Spontaneous construction of nucleophilic carbonyl-containing interphase toward ultrastable zinc-metal anodes, Adv. Mater. 34 (33) (2022), 2202733, https://doi.org/10.1002/adma.202202733.

[27] L.T. Hieu, S. So, I.T. Kim, J. Hur, Zn anode with flexible β-PVDF coating for aqueous Zn-ion batteries with long cycle life, Chem. Eng. J. 411 (2021), 128584, https://doi.org/10.1016/j.cej.2021.128584.

[28] W. Du, E.H. Ang, Y. Yang, Y. Zhang, M. Ye, C.C. Li, Challenges in the material and structural design of zinc anode towards high-performance aqueous zinc-ion batteries, Energy Environ. Sci. 13 (10) (2020) 3330–3360, https://doi.org/10.1039/d0ee02079f.

[29] X. Zheng, T. Ahmad, W. Chen, Challenges and strategies on Zn electrodeposition for stable Zn-ion batteries, Energy Storage Mater. 39 (2021) 365–394, https://doi.org/10.1016/j.ensm.2021.04.027.

[30] Y. Zhang, X. Zheng, N. Wang, W.H. Lai, Y. Liu, S.L. Chou, H.K. Liu, S.X. Dou, Y. X. Wang, Anode optimization strategies for aqueous zinc-ion batteries, Chem. Sci. 13 (48) (2022) 14246–14263, https://doi.org/10.1039/d2sc04945g.
[31] J. Hao, X. Li, X. Zeng, D. Li, J. Mao, Z. Guo, Deeply understanding the Zn anode behaviour and corresponding improvement strategies in different aqueous Zn-based batteries, Energy Environ. Sci. 13 (11) (2020) 3917–3949, https://doi.org/10.1039/d0ee02162h.
[32] Y. Wang, X. Xu, J. Yin, G. Huang, T. Guo, Z. Tian, R. Alsaadi, Y. Zhu, H. N. Alshareef, MoS2 -mediated epitaxial plating of Zn metal anodes, Adv. Mater. 35 (6) (2023), 2208171, https://doi.org/10.1002/adma.202208171.
[33] J. Shi, T. Sun, J. Bao, S. Zheng, H. Du, L. Li, X. Yuan, T. Ma, Z. Tao, Water-in-deep eutectic solvent" electrolytes for high-performance aqueous Zn-ion batteries, Adv. Funct. Mater. 31 (23) (2021), 2102035, https://doi.org/10.1002/adfm.202102035.
[34] K. Wu, J. Yi, X. Liu, Y. Sun, J. Cui, Y. Xie, Y. Liu, Y. Xia, J. Zhang, Regulating Zn deposition via an artificial solid-electrolyte interface with aligned dipoles for long life Zn anode, Nano Micro Lett. 13 (1) (2021), 79, https://doi.org/10.1007/s40820-021-00599-2.
[35] R. Yan, W. He, T. Zhai, H. Ma, Corrosion protective performance of amino trimethylene phosphonic acid-metal complex layers fabricated on the cold-rolled steel substrate via one-step assembly, Appl. Surf. Sci. 442 (2018) 264–274, https://doi.org/10.1016/j.apsusc.2018.02.167.
[36] S. Chen, Q. Chen, J. Ma, J. Wang, K.S. Hui, J. Zhang, Interface coordination stabilizing reversible redox of zinc for high-performance zinc-iodine batteries, Small 18 (22) (2022), 2200168, https://doi.org/10.1002/smll.202200168.
[37] R. Yuksel, O. Buyukcakir, W.K. Seong, R.S. Ruoff, Metal-organic framework integrated anodes for aqueous zinc-ion batteries, Adv. Energy Mater. 10 (16) (2020), 1904215, https://doi.org/10.1002/aenm.201904215.
[38] M. Liu, J. Cai, H. Ao, Z. Hou, Y. Zhu, Y. Qian, $NaTi_2(PO_4)_3$ solid-state electrolyte protection layer on Zn metal anode for superior long-life aqueous zinc-ion batteries, Adv. Funct. Mater. 30 (50) (2020), 2004885, https://doi.org/10.1002/adfm.202004885.
[39] H. Hu, J. Saniger, J. Garcia-Alejandre, V.M. Castaño, Fourier transform infrared spectroscopy studies of the reaction between polyacrylic acid and metal oxides, Mater. Lett. 12 (4) (1991) 281–285.
[40] J. Dong, Y. Ozaki, K. Nakashima, Infrared, Raman, and near-infrared spectroscopic evidence for the coexistence of various hydrogen-bond forms in poly(acrylic acid), Macromolecules 30 (4) (1997) 1111–1117, https://doi.org/10.1021/ma960693x.
[41] Y. Lv, M. Zhao, Y. Du, Y. Kang, Y. Xiao, S. Chen, Engineering a self-adaptive electric double layer on both electrodes for high-performance zinc metal batteries, Energy Environ. Sci. 15 (11) (2022) 4748–4760, https://doi.org/10.1039/d2ee02687b.
[42] H. Tian, J.L. Yang, Y. Deng, W. Tang, R. Liu, C. Xu, P. Han, H.J. Fan, SteeL anti-corrosion strategy enables long-cycle Zn anode, Adv. Energy Mater. 13 (1) (2022), 2202603, https://doi.org/10.1002/aenm.202202603.
[43] Y. Xie, J. Huang, T. Kong, X. Zhou, K. Wu, X. Liu, J. Yi, L. Xing, Y. Xia, Moisture-activated deep eutectic electrolyte enabling stable metal Zn anode, Energy Storage Mater. 56 (2023) 218–226, https://doi.org/10.1016/j.ensm.2023.01.013.
[44] H. Fan, M. Li, E. Wang, Anion-functionalized interfacial layer for stable Zn metal anodes, Nano Energy 103 (2022), 107751, https://doi.org/10.1016/j.nanoen.2022.107751.
[45] P. Liang, J. Yi, X. Liu, K. Wu, Z. Wang, J. Cui, Y. Liu, Y. Wang, Y. Xia, J. Zhang, Highly reversible Zn anode enabled by controllable formation of nucleation sites for Zn-based batteries, Adv. Funct. Mater. 30 (13) (2020), 1908528, https://doi.org/10.1002/adfm.201908528.